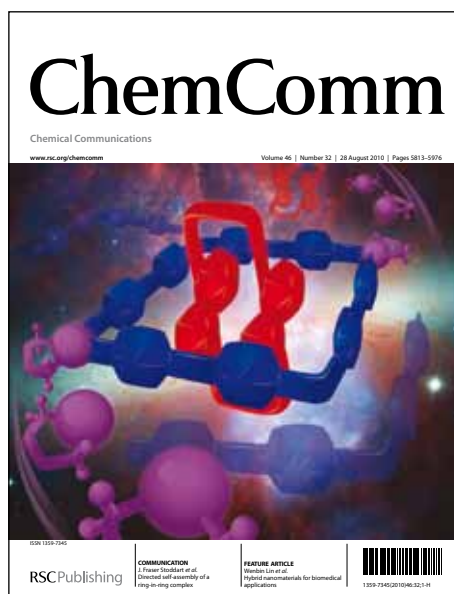


# ChemComm

## Accepted Manuscript



This is an *Accepted Manuscript*, which has been through the RSC Publishing peer review process and has been accepted for publication.

*Accepted Manuscripts* are published online shortly after acceptance, which is prior to technical editing, formatting and proof reading. This free service from RSC Publishing allows authors to make their results available to the community, in citable form, before publication of the edited article. This *Accepted Manuscript* will be replaced by the edited and formatted *Advance Article* as soon as this is available.

To cite this manuscript please use its permanent Digital Object Identifier (DOI®), which is identical for all formats of publication.

More information about *Accepted Manuscripts* can be found in the [Information for Authors](#).

Please note that technical editing may introduce minor changes to the text and/or graphics contained in the manuscript submitted by the author(s) which may alter content, and that the standard [Terms & Conditions](#) and the [ethical guidelines](#) that apply to the journal are still applicable. In no event shall the RSC be held responsible for any errors or omissions in these *Accepted Manuscript* manuscripts or any consequences arising from the use of any information contained in them.

# Synthesis of Hierarchically Structured ZnO Nanomaterials via Supercritical Assisted Solvothermal Process

Meng Wang<sup>a</sup>, Bin Zhao<sup>b,\*</sup>, Shaohong Xu<sup>b</sup>, Lin Lin<sup>b</sup>, Sijun Liu<sup>b</sup>, Dannong He<sup>a,b,\*</sup>

Received (in XXX, XXX) Xth XXXXXXXXXX 200X, Accepted Xth XXXXXXXXXX 200X

First published on the web Xth XXXXXXXXXX 200X

DOI: 10.1039/b000000x

**Hierarchically structured ZnO nanomaterials with flower-sheet-particle morphologies were synthesized via supercritical assisted solvothermal process free from any other auxiliary chemicals.**

Recently, zinc oxide (ZnO) nanomaterials have attracted considerable attentions owing to their excellent optical, electrical and catalytic properties.<sup>1</sup> These low cost and environmentally friendly nanostructures with a wide band gap (3.37 eV) have been considered for extensive applications, such as photocatalyst, hydrogen generation, solar cell, gas sensor, antibiosis and so on.<sup>2</sup> Several methods were reported to synthesize zinc oxide including solution-based reaction, homogeneous precipitation, calcination, solvothermal treatment, Sol-Gel, microwave, ultrasonic and even biological method.<sup>1-3</sup> Among them the solvothermal and calcination treatments were most commonly used to synthesize ZnO nanomaterials. But these methods might result in the excessive growth of crystalline grain<sup>2b</sup> and might cause the environmental/product pollution because of the additions of some organic (e.g. Hexamethylenetetramine,<sup>1e, 2b</sup> Trizma base,<sup>2a</sup> etc.) and inorganic auxiliary chemicals (e.g. Trisodium citrate,<sup>2d</sup> NH<sub>3</sub>,<sup>1e, 3d</sup> etc.). So it is still significant to develop novel green routes to synthesize highly dispersed ZnO nanomaterials.

Recently, a new approach has attracted much attention to synthesize inorganic oxide nanomaterials using supercritical fluids.<sup>4</sup> Supercritical technology is a very green route which can avoid the contamination of products. In recent years, several works reported the synthesis of ZnO nanomaterials using supercritical water.<sup>4b</sup> However, synthesis of ZnO nanomaterials via a supercritical CO<sub>2</sub> (ScCO<sub>2</sub>) assisted solvothermal process free from any auxiliary chemicals has been rarely reported to date, although ScCO<sub>2</sub> has several advantages such as non-flammability, relative inertness, complete miscibility with gases, and easy separation from liquid/solid products after reactions.<sup>5</sup>

In this work, hierarchically structured ZnO nanomaterials with flower-sheet-particle morphologies were obtained via ScCO<sub>2</sub> assisted solvothermal process combined with the calc-

ination treatment, which was free from any organic/ inorganic auxiliary chemicals. The supercritical fluid apparatus is schematically shown in Fig. S1 (ESI†). In a typical procedure, 5.0g zinc nitrate hexahydrate Zn(NO<sub>3</sub>)<sub>2</sub>·6H<sub>2</sub>O was dissolved into 20 ml deionized water. After stirring for a short time the resulting transparent solution was transferred into the reactor A41 (Fig. S1, ESI†). Then the reactor A41 was heated to 120 °C for 24 h in the ScCO<sub>2</sub> pressure of 200 bar. After the reaction the powdery product was obtained and directly dried by ScCO<sub>2</sub> fluid and CO<sub>2</sub> gas flow. Before characterizations the as-prepared product was collected and calcined at 200 °C, 400 °C and 600 °C for 2 h in the air, respectively.

XRD pattern shown in Fig. S2a (ESI†) indicates the as-prepared product of hydrozincite Zn<sub>5</sub>(CO<sub>3</sub>)<sub>2</sub>(OH)<sub>6</sub> obtained under supercritical CO<sub>2</sub> assisted solvothermal treatment. The corresponding FESEM images of as-prepared product are shown in Figs. 1a and 1b, in which its morphology just like the flower clusters with the size of about 1 μm. An entire cluster of hydrozincite nanoflower shown in Fig. 1b indicates the hierarchical structure composed of nanosheets less than 50 nm thick. The XRD pattern of calcined product obtained at 200 °C (Fig. S2b, ESI†) shows the coexistence of hydrozincite and ZnO, indicating the intermediate condition of phase transition process. The corresponding SEM images (Figs. 1c and 1d) exhibit the product also maintains the flower-like morphologies, but a great amount of cracks are formed on the nanosheets, showing the embryonic profiles of nanoparticles. XRD pattern shown in Fig. S2c (ESI†) indicates the product of zincite ZnO obtained by calcining the as-prepared product at 400 °C for 2 h. Consequently, the SEM images shown in Figs. 1e and 1f give typical images of hierarchically structured ZnO nanomaterials with flower-sheet-particle morphologies. The ZnO nanosheets are definitely different from hydrozincite nanosheets, which is clearly shown in Fig. 1f indicating a fragmentation process occurred from smooth

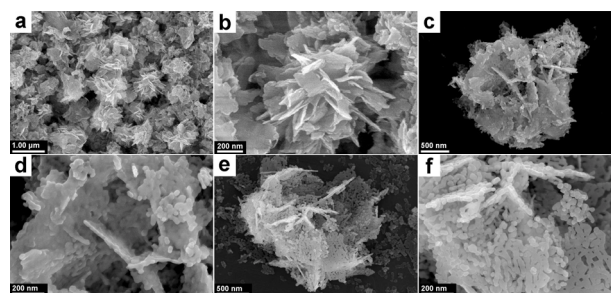


**Fig. 1** FESEM images of the as-prepared uncalcined product (a, b) and calcined products obtained at 200 °C (c, d) and 400 °C (e, f), respectively.

<sup>a</sup> School of Materials Science and Engineering, Shanghai JiaoTong University, 800 Dongchuan Road, Shanghai 200240, China.

<sup>b</sup> National Engineering Research Center for Nanotechnology, 28 East Jiangchuan Road, Shanghai 200241, China.

\* Corresponding authors. E-mail addresses: zhaobinwily@hotmail.com; dannonghe@126.com. Tel.: +86-21-34291286; Fax: +86-21-34291125.

Electronic Supplementary Information (ESI) available: Supercritical apparatus, XRD, Raman, TG-DSC and BET analysis for the products. See DOI: 10.1039/b000000x/

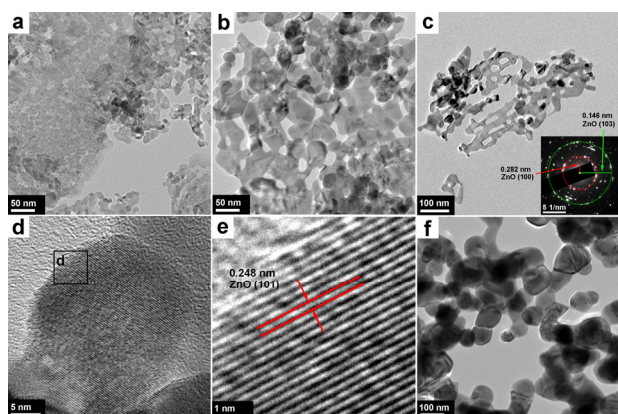


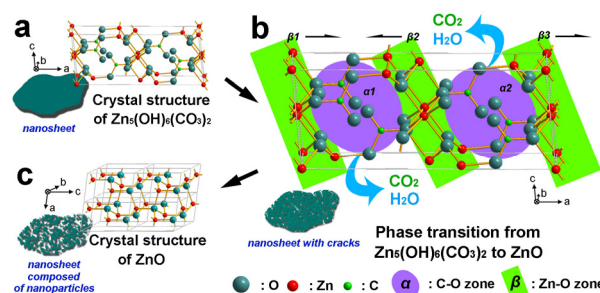
**Fig. 2** TEM and HRTEM images of the calcined products obtained at 200 (a), 400 (b-e) and 600 °C (f) for 2 h. The bottom right inset in Fig. 2c is the corresponding SAED pattern.

hydrozincite nanosheets to sub-hierarchically structured ZnO nanosheets composed of nanoparticles.

TEM image of calcined product obtained at 200 °C (Fig. 2a) shows the rough morphologies of nanosheets distributed by a lot of cracks. TEM images of ZnO nanosheets obtained at 400 °C (Figs. 2b and 2c) exhibit a great amount of mesoporous holes with the pore size of about 10-30 nm through the ZnO nanosheet, indicating the formation of hierarchically structured ZnO nanosheets composed of nanoparticles. The corresponding SAED pattern located in the bottom right inset in Fig. 2c indicates the nanocrystalline state of the product, and the red and green diffraction rings correspond well with the (100) and (103) lattice planes of zincite ZnO, respectively. The HRTEM image of Fig. 2d shows that a pure single ZnO nanoparticle with the particle size of about 30 nm exhibits the perfect lattice planes. The marked area is further magnified in the HRTEM image of Fig. 2e, where the clear lattice fringes should correspond with the (101) planes of zincite ZnO. Fig. 3f shows the particles with the size of about 100 nm, indicating an excessive growth of ZnO particle at the calcined temperature of 600 °C.

In addition, Raman spectras (Fig. S3, ESI†) also indicate the phase transition from hydrozincite to ZnO and the crystalline growth of ZnO nanoparticles with the elevation of calcined temperatures, which correspond well with the XRD results. A TG-DSC analysis (Fig. S4, ESI†) was carried out to investigate the thermal conversion characteristics of the as-prepared hydrozincite. The endothermic peak centered at around 250.8 °C should be attributed to the decomposition of hydrozincite by release of water and carbon dioxide.

The formation mechanism for the hierarchically structured ZnO nanomaterials is proposed in Scheme 1, according to the Gibbs-Curie-Wulff theorem<sup>6</sup> combined with the BET and BJH analysis (Fig. 3) and the experimental results above. In the  $ScCO_2$  fluid assisted solvothermal process, Zn species are reacted with  $H_2O$  and high pressured  $CO_2$  to create hydrozincite (Scheme 1a). Recently, several works reported that a number of highly dispersed, porous or hierarchically structured materials of metal oxides were prepared with the assistance of  $ScCO_2$ .<sup>4,7</sup> The  $ScCO_2$  fluids show low viscosity and high diffusivity and never condense into the liquid phase above the critical temperature,<sup>7d</sup> which could probably offer



**Scheme 1** Schematic drawing of the phase transition behavior from hydrozincite to ZnO and the formation mechanism of hierarchically structured ZnO nanomaterials.

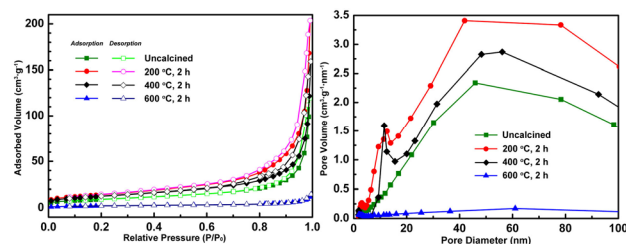


**Fig. 3**  $N_2$  adsorption/desorption isotherms (a) and pore size distributions (b) for as-prepared uncalcined product and calcined products obtained at 200 °C, 400 °C and 600 °C, respectively.

specific advantages for the formation of highly incompact hierarchically structured hydrozincite nanoflowers assembled by nanosheets. The green curve in Fig. 3b shows the uncalcined product contains a somewhat high proportion of porous distribution with the diameters > 20 nm, which should be produced by the unique morphologies of nanosheets assembled hydrozincite nanoflowers.

In the phase transition process (Scheme 1b), the cleavages of Zn-O bonds in Zn-O-C chains and the dehydration between -OH groups probably result in the generations of  $CO_2$  and  $H_2O$  in C-O zones. At the same time, a large amount of vacancies should be formed accompanied by the formations of new Zn-O bonds as the result of the generations of  $CO_2$  and  $H_2O$  escaping from the crystalline structure of hydrozincite, and the expansion of vacancies may result in the formation of cracks and mesoporous holes at the nanosheets in the phase transition process. SEM and TEM images of calcined products at 200 °C (Figs. 1c, 1d, 2a) give the clear nanosheets distributed by a lot of cracks, which correspond well with the proposed hypothesis above. The red curve in Fig. 3b shows the calcined product obtained at 200 °C contains not only a high proportion of broad porous distribution with diameters > 20 nm but also a weak mesoporous peak centered at about 12 nm. This weak peak is probably assigned to the cracks and a small amount of mesoporous holes at the nanosheets formed in the phase transition process.

This phase transition and morphological evolution process should be governed by the Gibbs-Curie-Wulff theorem.<sup>6a</sup> At the initial stages of the reaction in nonequilibrium growth conditions, the crystalline phase of the seeds is critical for directing the intrinsic shapes of the crystals due to its characteristic symmetry and structure. At the final stages, the growth process shifts into the thermo dynamic equilibrium regime.<sup>6b</sup> Therefore, the phase transition from hydrozincite to

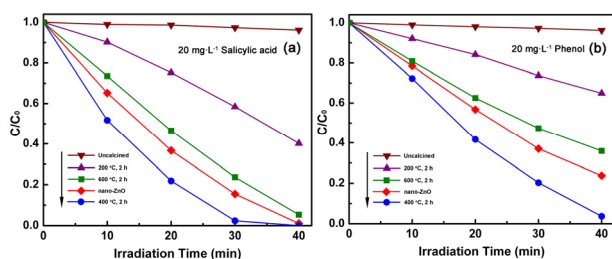


**Fig. 4** Photocatalytic degradation of salicylic acid (a) and phenol (b) solution under UV irradiation. (nano-ZnO: commercial ZnO nanoparticles)

ZnO is faster and further complete at a higher temperature of 400 °C (Scheme 1c), while the cracks are further expanded and the ZnO nanoparticles with more distinct profiles are formed in order to decrease the surface energy. In addition, CO<sub>2</sub> molecules may be adsorbed by hydroxyl (-OH) groups located on the surface of hydrozincite nanosheets. These adsorbed CO<sub>2</sub> molecules from ScCO<sub>2</sub> process could probably maintain the nanosheets assembled frameworks during the phase transition process. The black curve in Fig. 3b shows the calcined product obtained at 400 °C contains not only a high proportion of broad porous distribution with diameters > 20 nm but also an obvious narrow mesoporous peak centered at about 12 nm, which should be assigned to the large amount of mesoporous holes at the nanosheets accumulated by ZnO nanoparticles as well as the formation of hierarchically structured ZnO nanomaterial with flower-sheet-particle morphologies. Finally, the pore size distribution of the calcined product obtained at 600 °C (Fig. 3b, blue curve) shows a very weak porous distribution, which indicates the collapse of the hierarchical ZnO structure. The BET and BJH analysis correspond well with the results of SEM and TEM characterizations.

Fig. 4 shows the photoactivities of the products evaluated via bleaching 20 mg·L<sup>-1</sup> salicylic acid (a) and phenol (b) solutions under UV irradiation (300 W). The hydrozincite and hydrozincite-contained product show lower photoactivity. The pure ZnO products (obtained at 400 and 600 °C) exhibit high photoactivities. The corresponding initial rate constants of the ZnO nanomaterials obtained at 400 °C calculated according to the pseudo-first-order reaction are  $6.60 \times 10^{-2}$  (salicylic acid) and  $3.25 \times 10^{-2}$  (phenol) min<sup>-1</sup>, respectively, which are the highest photoactivities in this work and obviously higher than that of the commercial ZnO nanoparticles (Aladdin Reagent, 30±10 nm). The high photoactivity is probably due to its special hierarchical structure which may provide more free surface charges carriers in the photodegradation process.<sup>8</sup>

In summary, hierarchically structured ZnO nanomaterials with flower-sheet-particle morphologies were obtained via ScCO<sub>2</sub> assisted solvothermal process combined with the calcination treatment. A formation mechanism governed by Gibbs-Curie-Wulff theorem was proposed based on our experimental results, in which the XRD, Raman and TG-DSC characterizations were used to analyze the phase transition behavior from hydrozincite to ZnO, and the SEM, TEM and BET methods were employed to clearly elucidate the morphological evolution from hydrozincite nanoflowers to hierarchically structured ZnO nanomaterials with flower-

sheet-particle morphologies, which revealed that the expansion of vacancies accompanied by the creations of new Zn-O bonds could result in the formation of cracks and mesoporous holes at the nanosheets in the phase transition process. The hierarchical ZnO product shows excellent photoactivity in the photodegradation of salicylic acid and phenol solutions under UV light irradiation.

This work was supported by the Research Programs of Shanghai Science and Technology Committee (11520706100, 13NM1401600), Shanghai Rising-Star Program (B-type) (12QB1402800) and the National High Technology Research and Development Program of China (863 Program, 2013AA031801).

## Notes and references

- (a) A. Kelchtermans, K. Elen, K. Schellens, B. Conings, H. Damm, H.-G. Boyen, J. D'Haen, P. Adriaenssens, A. Hardy and M. K. Van Bael, *RSC Adv.*, 2013, **3**, 15254; (b) P. Li, Z. Wei, T. Wu, Q. Peng and Y. D. Li, *J. Am. Chem. Soc.*, 2011, **133**, 5660; (c) X. H. Lu, G. M. Wang, S. L. Xie, J. Y. Shi, W. Li, Y. X. Tong and Y. Li, *Chem. Commun.*, 2012, **48**, 7717; (d) S. G. Meng, D. Z. Li, X. Z. Zheng, J. X. Wang, J. Chen, J. L. Fang, Y. Shao and X. Z. Fu, *J. Mater. Chem. A*, 2013, **1**, 2744; (e) S. Kim, C.-H. Kim, S. K. Lee, J.-H. Jeong, J. Lee, S.-H. Jin, W. S. Shin, C. E. Song, J.-H. Choi and J.-R. Jeong, *Chem. Commun.*, 2013, **49**, 6033.
- (a) R. Boppella, K. Anjaneyulu, P. Basak and S.V. Manorama, *J. Phys. Chem. C*, 2013, **117**, 4597; (b) R. J. Zou, G. J. He, K. B. Xu, Q. Liu, Z. Y. Zhang and J. Q. Hu, *J. Mater. Chem. A*, 2013, **1**, 8445; (c) F. H. Chu, C. W. Huang, C. L. Hsin, C. W. Wang, S. Y. Yu, P. H. Yeh and W. W. Wu, *Nanoscale*, 2012, **4**, 1471; (d) Z. B. Yu, Y. P. Xie, G. Liu, G. Q. Lu, X. L. Ma and H. M. Cheng, *J. Mater. Chem. A*, 2013, **1**, 2773; (e) X. L. Wang, F. Yang, W. Yang and X. R. Yang, *Chem. Commun.*, 2007, 4419. (f) A. Pang, C. Chen, L. Chen, W. Liu and M. Wei, *RSC Adv.*, 2012, **2**, 9565; (g) Q. Zhang, T. P. Chou, B. Russo, S. A. Jenekhe and G. Cao, *Angew. Chem. Int. Ed.*, 2008, **47**, 2402.
- (a) S. Cho, J. W. Jang, J. Kim, J. S. Lee, W. Choi and K. H. Lee, *Langmuir*, 2011, **27**, 10243; (b) L. Y. Zhang, L. W. Yin, C. X. Wang, N. Lun and Y. X. Qi, *ACS Appl. Mater. Inter.*, 2010, **2**, 1769; (c) D. Ledwith, S. C. Pillai, G. W. Watson and J. M. Kelly, *Chem. Commun.*, 2004, 2294; (d) S. S. Warule, N. S. Chaudhari, B. B. Kale and M. A. More, *CrystEngComm*, 2009, **11**, 2776.
- (a) M. Chatterjee, T. Ishizaka, T. Suzuki, A. Suzuki and H. Kawanami, *Green Chem.*, 2012, **14**, 3415; (b) A. Leybros, R. Piolet, M. Ariane, H. Muhr, F. Bernard and F. Demoisson, *J. Supercrit. Fluids*, 2012, **70**, 17; (c) M. Wei, K. Wang, M. Yanagida, H. Sugihara, M. A. Morris, J. D. Holmes and H. Zhou, *J. Mater. Chem.*, 2007, **17**, 3888.
- (a) R. P. Marin, S. A. Kondrat, R. K. Pinnell, T. E. Davies, S. Golunski, J. K. Bartley, G. J. Hutchings and S. H. Taylor, *Appl. Catal. B, Environ.*, 2013, **140**, 671; (b) M. Wang, C. Chen, B. Zhao, Q. Q. Zeng and D. N. He, *Mater. Lett.*, 2013, **109**, 104; (c) H. Monhemi, M. R. Housaindokht, M. R. Bozorgmehr and M. S. S. Googheri, *J. Supercrit. Fluids*, 2012, **69**, 1.
- (a) J. W. Mullin, *Crystallization*, 4th Ed. Butterworth Heinemann, Boston, 2001; (b) X. Ge, S. Y. Song and H. J. Zhang, *CrystEngComm*, 2012, **14**, 7306; (c) S. Y. Gao, J. M. Yang, Z. D. Li, X. X. Jia and Y. L. Chen, *J. Hazard. Mater.*, 2012, **211**, 55.
- (a) B. J. Liu, A. G. Wong-Foy and A. J. Matzger, *Chem. Commun.*, 2013, **49**, 1419; (b) R. K. Totten, Y.-S. Kim, M. H. Weston, O. K. Farha, J. T. Hupp and S. T. Nguyen, *J. Am. Chem. Soc.*, 2013, **135**, 11720; (c) R. A. Pai, R. Humayun, M. T. Schulberg, A. Sengupta, J. N. Sun and J. J. Watkins, *Science*, 2004, **303**, 507; (d) K. Matsuyama, K. Mishima, T. Kato and K. Ohara, *Ind. Eng. Chem. Res.*, 2010, **49**, 8510.
- C. Z. Wu, L. Y. Lei, X. Zhu, J. L. Yang and Y. Xie, *Small*, 2007, **3**, 1518-1522.